nature chemistry

SUPPLEMENTARY INFORMATION

https://doi.org/10.1038/s41557-018-0166-9

In the format provided by the authors and unedited.

Prevention of dendrite growth and volume expansion to give high-performance aprotic bimetallic Li-Na alloy–O_2 batteries

Jin-ling Ma[1,2,3], Fan-lu Meng[2], Yue Yu[1,4], Da-peng Liu[5], Jun-min Yan[2]*, Yu Zhang[5,6,7]*, Xin-bo Zhang[1]* and Qing Jiang[2]

[1]State Key Laboratory of Rare Earth Resource Utilization, Changchun Institute of Applied Chemistry, Chinese Academy of Sciences, Changchun, China. [2]Key Laboratory of Automobile Materials, Ministry of Education, and Department of Materials Science and Engineering, Jilin University, Changchun, Jilin, China. [3]University of Chinese Academy of Sciences, Beijing, China. [4]University of Science and Technology of China, Hefei, Anhui, China. [5]Key Laboratory of Bio-Inspired Smart Interfacial Science and Technology of Ministry of Education School of Chemistry Beihang University Beijing, Beijing, China. [6]International Research Institute for Multidisciplinary Science Beihang University Beijing, Beijing, China. [7]Beijing Advanced Innovation Center for Biomedical Engineering Beihang University Beijing, Beijing, China. *e-mail: junminyan@jlu.edu.cn; jade@buaa.edu.cn; xbzhang@ciac.ac.cn

Table of Contents

Experiment Methods:

1. Chemicals and Materials

Sodium (Na, > 99.5%, Sinopharm Chemical Reagent Co., Ltd), lithium (Li, > 99.9%, Shanghai Shunyun Metal Material Co., Ltd.), sodium trifluoromethanesulfonate ($NaCF_3SO_3$, Sigma-Aldrich), tetraethylene glycol dimethyl ether (TEGDME, Sigma-Aldrich), anhydrous *n*-hexane (C_6H_{14}, Aladdin Reagent), 1,3-dioxolane (DOL, 99%, Sigma-Aldrich), diethylamine ($C_4H_{11}N$, Aladdin Reagent), ruthenium(III) chloride hydrate ($RuCl_3 \cdot xH_2O$, Aladdin Reagent), polyacrylonitrile (PAN, Mw = 150 K, J&K Co), cobalt(III) acetylacetonate ($Co(Acac)_3$, 97%, Aladdin Reagent), cellulose acetate (CA, Aladdin Reagent), N,N-dimethylformanide (99.5%, DMF, Macklin Reagent), lithium triflate ($LiCF_3SO_3$, 98%, Macklin Reagent), carbon paper (CP, TGP-H-060, Toray), polyvinylidene fluoride (PVDF, Mw = 534,000, Sigma-Aldrich), and multiwalled carbon nanotubes (CNTs, Cnano Technology Ltd. Co.).

2. Li–Na Alloy Anode Preparation

A dry lithium plate and clean sodium strip were cut into pieces and then put into a self-made container. The lithium plate and sodium pieces were melted by heating the container and stirred to ensure even dispersion. The alloy ingots were then cooled to room temperature. All of the aforementioned operations were carried out in an Ar-filled glove box (**Supplementary Table 1)**.

3. RuO_2/CNTs Catalyst Preparation

Eighty milligrams of CNT powder were dispersed in 40 mL of diethylamine, and the resultant mixture was stirred vigorously. Subsequently, 180 mg of ruthenium chloride hydrate was added to the suspension and the resultant mixture stirred for another 4 h. Finally, the suspension was transferred to an autoclave vessel and was bubbled with O_2 before the vessel was sealed. The vessel was heated at 200 °C for 4 h and cooled quickly in an ice bath. The generated RuO_2/CNTs were washed with distilled water and ethanol separately three times. Finally, the obtained RuO_2/CNT powder with a 21% RuO_2 loading was dried at 80 °C overnight.

4. Co/N-doped Carbon Fibers (Co/NCF) Preparation

The precursor solution for electrospinning was first prepared by dissolving 0.6 g of polyacrylonitrile (PAN, Mw = 150 000) and 0.6 g of cellulose acetate in 10 mL of N,N-dimethylformamide (DMF) with vigorous stirring for 5 h. Then, 0.5 g of $Co(Acac)_3$ was added into the solution and stirred overnight at room temperature. After that, the above mixture was transferred to a plastic syringe equipped with a 9-gauge stainless steel nozzle made. The distance between the needle tip and the collector was 16 cm and the flow rate of the syringe pump was 1.0 mL h^{-1}. The voltage was conducted at 20 kV and a sprayed dense web of fibers was collected on the aluminum foil. The resultant polymer nanofiber films were carefully cut out according to the requirement and stabilized at 280 °C in air for 2 h with the heating rate of 1 °C min^{-1}. Next, the prepared polymer nanofiber film was placed into a porcelain boat with ~2 g of melamine (the weight ratio of melamine and the sample is 10:1) paved under the film. The mixture was calcined at 750 °C for 2 h with a heating rate of 5 °C min^{-1} under the protection of Ar.

5. Li|Li, Li-Na alloy|Li-Na alloy, and Na|Na Symmetric Batteries for Galvanostatic Test

Two foils of the same metal (Li, Li-Na alloy, or Na) with a thickness of 0.15 mm were used as the working electrode and counter/reference electrode, respectively. The separator was sandwiched between the two electrodes and assembled into a CR2025-type coin battery with the electrolyte. Two different electrolytes were used: 0.5 M sodium trifluoromethanesulfonate ($NaCF_3SO_3$) in tetraethylene glycol dimethyl ether (TEGDME), and 0.5 M $NaCF_3SO_3$ in TEGDME and 1,3-dioxolane (DOL) (volume ratio 1:1) (H_2O < 10 ppm). Galvanostatic tests were carried out by stripping and depositing in each cycle for 2 h under a constant current density using a LAND CT2001A multichannel battery testing system. Electrochemical impedance spectroscopy (EIS) was carried out at room temperature using an AC impedance analyzer on a Biologic VMP3 electrochemical workstation. Voltage profiles of metal | Cu were tested in three-electrode battery using lithium metal as the reference electrode in 0.5 M $NaCF_3SO_3$/DOL/TEGDME electrolyte.

6. Alloy-O_2 Battery Assembly and Electrochemical Tests

For cathode preparation, a pristine CNT cathode was prepared by casting homogenous ink composed of a mixture of 80 wt% CNT powder and 20 wt% PVDF binder onto the CP current collector. After casting, the cathodes were dried at 80 °C for 24 h under vacuum to remove residual solvent. For preparation of the RuO_2/CNT cathodes, CNT and RuO_2/CNTs powder were premixed in a 4:1 weight ratio. The active material loading (CNT or catalysts + CNT) was 0.6 mg cm^{-2}. The Co-N-CNT/CNF is binder-free cathode. All the batteries were assembled in an argon-filled glovebox using modified 2025-type coin batteries with ⌀2 mm holes in

their top cover to permit the diffusion of oxygen. A metal (Li-Na alloy, Li, or Na) anode (⌀12 mm, $0.1 \leq \delta \leq 0.2$ mm), a glass-fibre separator (⌀16 mm), the prepared CNTs or RuO_2/CNT cathode and 80 μL of electrolyte were combined in sequence. The assembled batteries were purified by the straight two-way piston conducted alternatively by vacuuming and ventilating three times with high-purity O_2. After that, the purified batteries were pumped into 250 mL O_2 and then were settled for 3 hours before electrochemical measurement. These metal-O_2 batteries were studied by cyclic voltammetry (CV) on a Biologic VMP3 electrochemical workstation at room temperature. CV was carried out at a scan rate of 0.1 mV s^{-1} in the range 1.9-4.2 V. The galvanostatic tests were conducted at a current density of 200 mA g^{-1} using a LAND CT2001A multichannel battery testing system. All the electrochemical tests were carried out in a chamber of pure O_2 (99.999%) at 1 atm.

7. Characterizations

For all of the characterizations after electrochemical tests, the batteries were disassembled in an argon-filled glove box (H_2O < 1 ppm, O_2 < 1 ppm), and the cathode and anode were washed with TEGDME. Then, the cathode and anode were washed with anhydrous acetonitrile and n-hexane respectively, and finally dried for 12 h in a glovebox. To characterize the morphological variation of the cathode and anode, scanning electron microscopy (SEM) was performed on a Hitachi S-4800 field-emission scanning electron microscope operating at an accelerating voltage of 10 kV. The home-made transparent battery was monitored using an Olympus DP73. Transmission electron microscopy (TEM) was performed using a FEI Tecnai G_2 S-Twin instrument with a field-emission gun operating at 200 kV. XRD patterns of the anode and cathode were obtained using an X-ray diffractometer (micro-XRD,

Rigaku, Japan). To avoid sample exposure to air and moisture during the XRD analysis, a homemade gas-tight XRD holder was used. The chemical compositions of the cycled anode were analysed by Fourier transform infrared spectroscopy (FTIR, Thermo fisher scientific, China), and X-ray photoelectron spectroscopy (XPS, Sigma probe, Thermo VG scientific, England) with an Mg Kα line as the X-ray source. A qualitative flame test was used to determine the presence of lithium and/or sodium on the discharged cathode. The discharge products from the discharged cathodes were initially dissolved in DI water, and then a platinum wire was immersed in the alkali-metal-ion-containing solution and finally placed into a blue flame. For all characterizations, moisture and air contamination of each sample were avoided by using an airtight sample box during the transfer process.

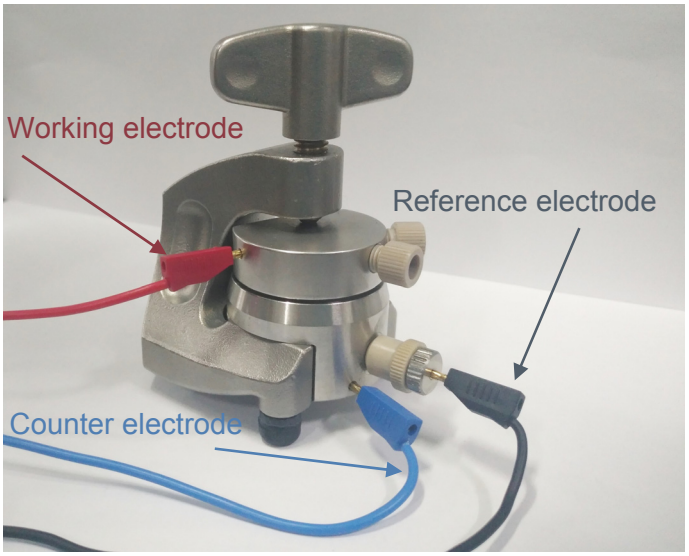

Supplementary Fig. 1. Three-electrode test device. The photograph of metal | Cu battery using Li as reference electrode.

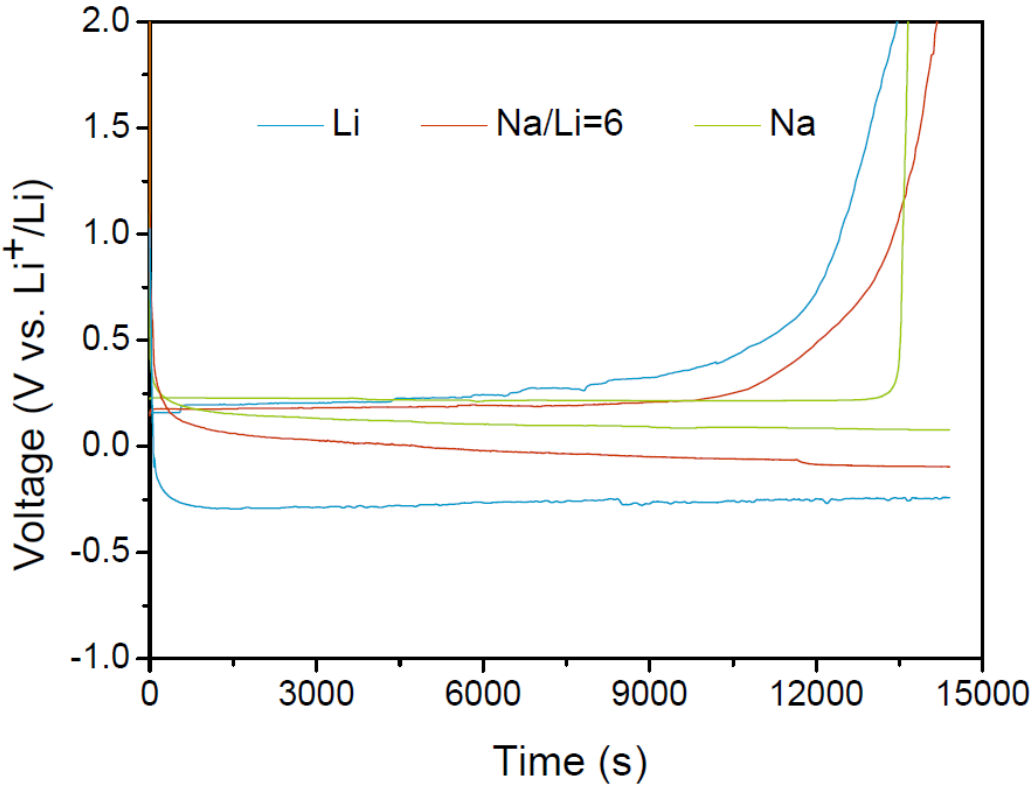

Supplementary Fig. 2. Voltage profiles of symmetric batteries using Li as a reference electrode. The stripping and platting curve of metal | Cu batteries tested with a Li reference electrode at a current density of 0.5 mA cm^{-2} for 4 h.

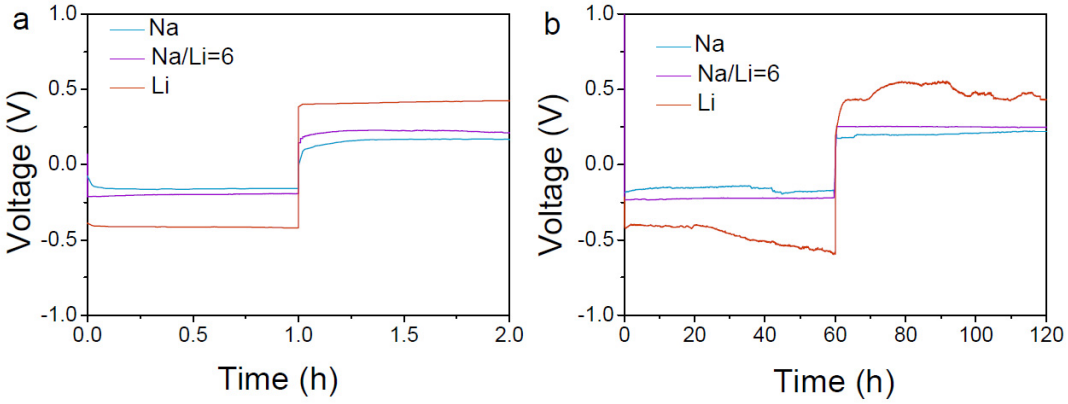

Supplementary Fig. 3. Voltage profiles of metal | metal symmetric batteries. Stripping and platting curves of Na | Na, Li-Na alloy | Li-Na alloy (Na/Li = 6), and Li | Li symmetric batteries in a) 2, and b) 120 h at a current density of 0.5 mA cm^{-2}.

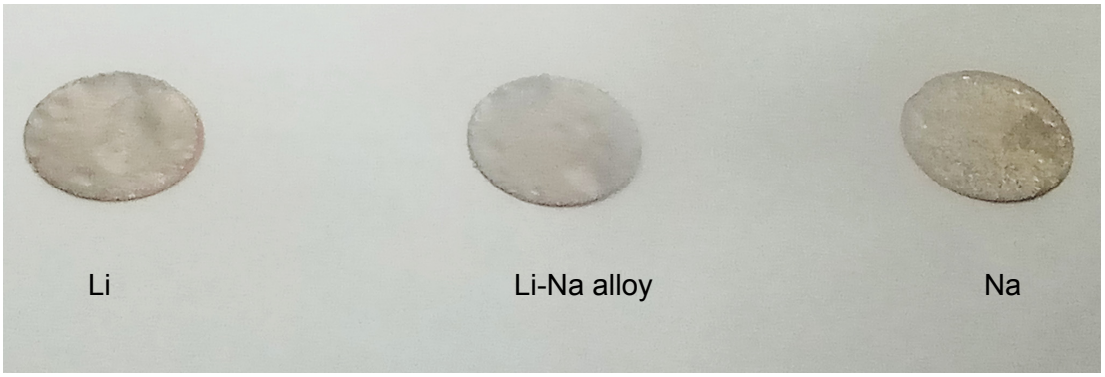

Supplementary Fig. 4. The photos of plated Li, Li-Na alloy, or Na metal on Cu foil. The plated capacity is 3 mAh cm^{-2} at a current density of 0.5 mA cm^{-2}.

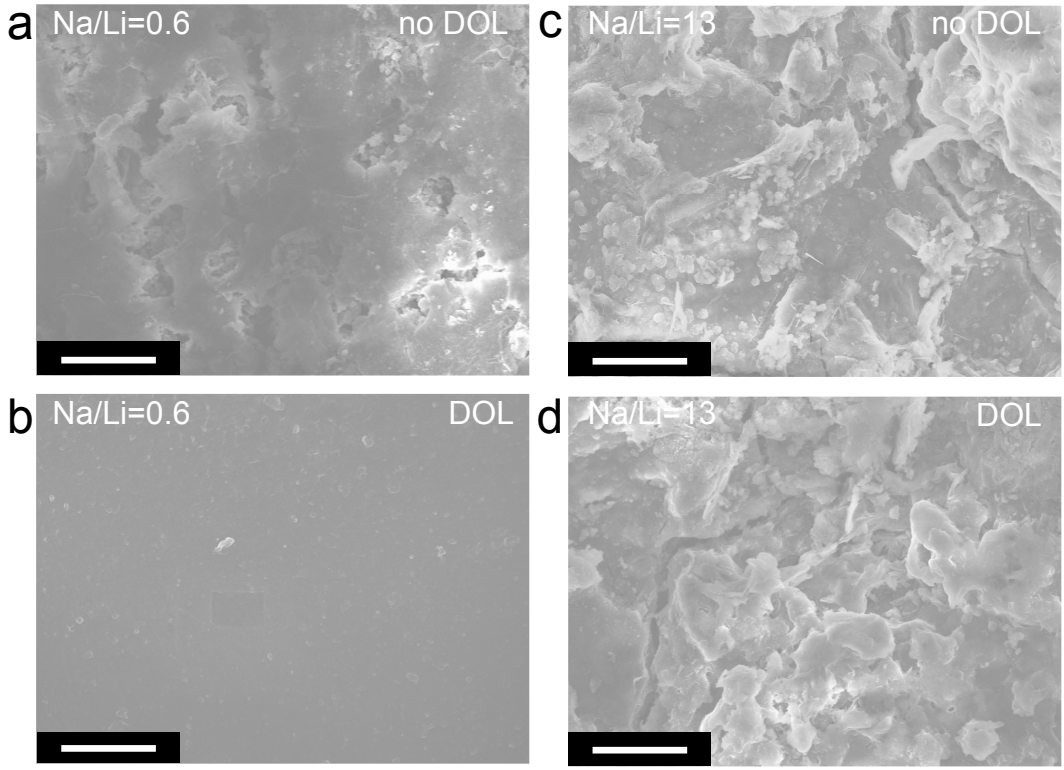

Supplementary Fig. 5. Effect of electrolyte on the morphology of cycled alloy electrodes. SEM images of electrodes after 5 cycles of stripping/plating with a capacity of 2 mAh cm^{-2} at a current density of 1 mA cm^{-2} in 0.5 M $NaCF_3SO_3$/TEGDME and $NaCF_3SO_3$/DOL/TEGDME electrolytes, respectively. Li-Na alloy with Na/Li of (**a**, **b**) 0.6, and (**c**, **d**) 13. Scale bar, 10 μm.

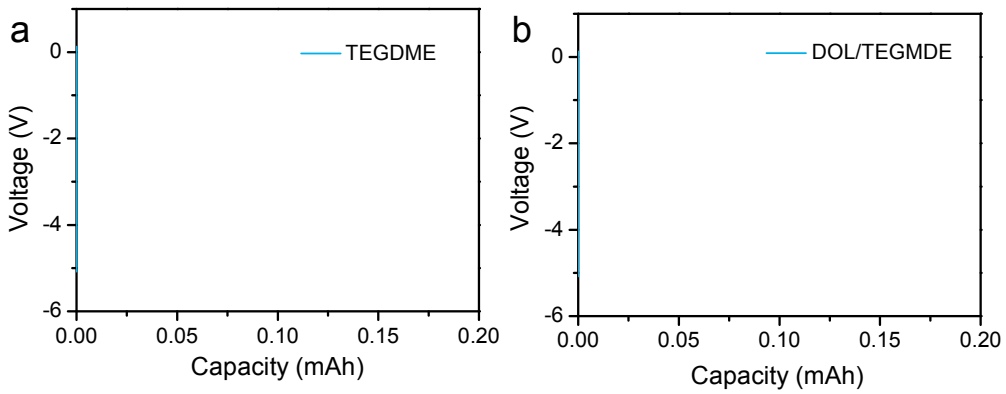

Supplementary Fig. 6. Voltage profiles of symmetric batteries in different solvents. Voltage profiles for Li-Na alloy | Li-Na alloy (Na/Li = 6) symmetric batteries in (**a**) TEGDME and (**b**) DOL/TEGDME solvents at a current density of 0.5 mA cm^{-2}.

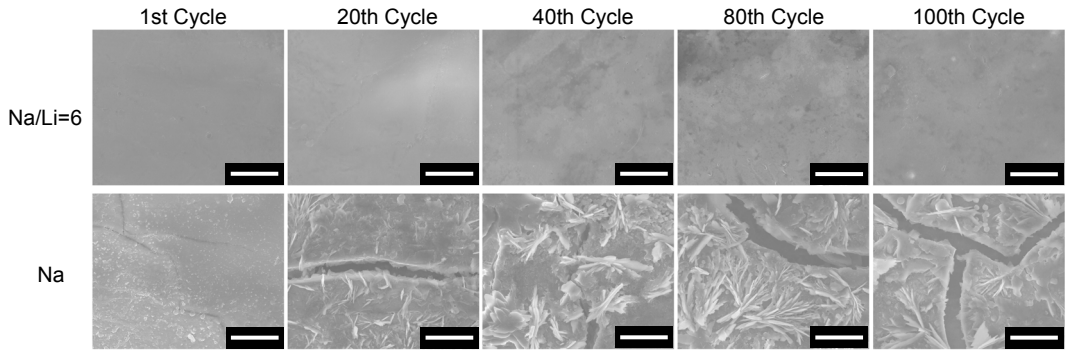

Supplementary Fig. 7. Morphology evolution of metal electrodes. SEM images of cycled alloy (Na/Li = 6) and Na electrodes corresponding to Figure 4b.

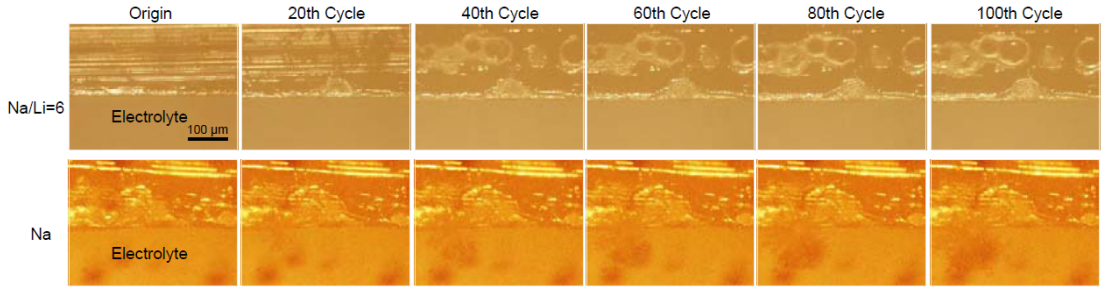

Supplementary Fig. 8. Morphology evolution of metal electrodes. *In situ* optical microscope images of cycled Li-Na alloy and Na electrode in symmetric battery (2 mA cm^{-2}, 8 min).

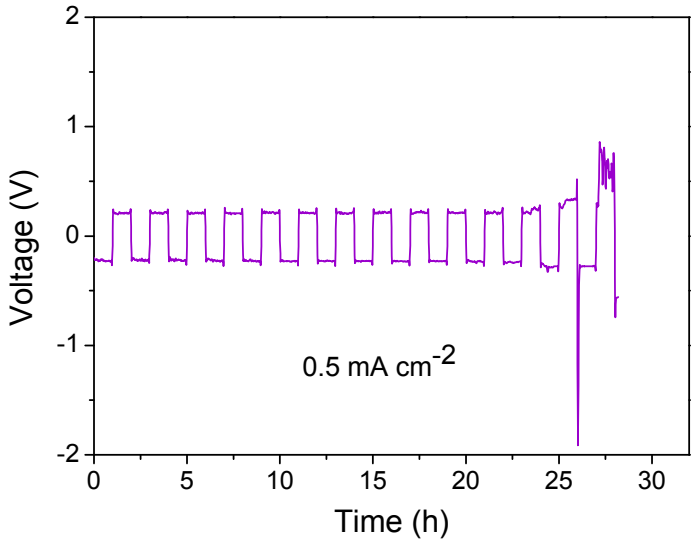

Supplementary Fig. 9. Voltage profiles of Na | Na symmetric batteries. Tested at a current density of 0.5 mA cm^{-2} in 0.5 M $NaCF_3SO_3$/DOL/TEGDME electrolyte containing 0.05 M Li^+.

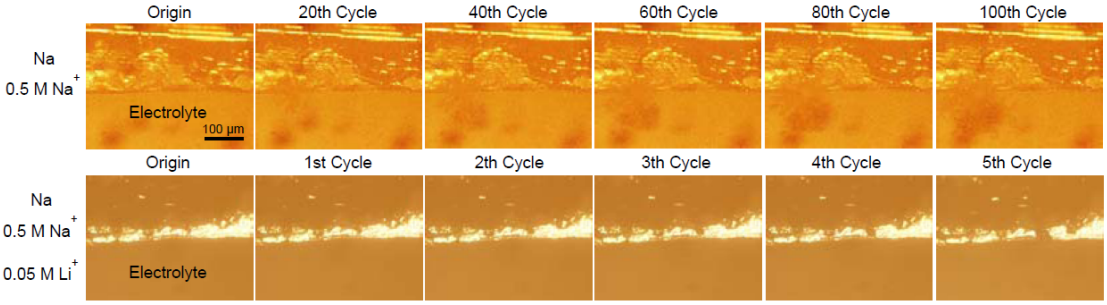

Supplementary Fig. 10. Morphology evolution of Na electrode. *In situ* optical microscope images of cycled Na electrode in symmetric battery containing 0.05 M and no Li^+ in 0.5 M $NaCF_3SO_3$/DOL/TEGDME electrolyte (2 mA cm^{-2}, 8 min).

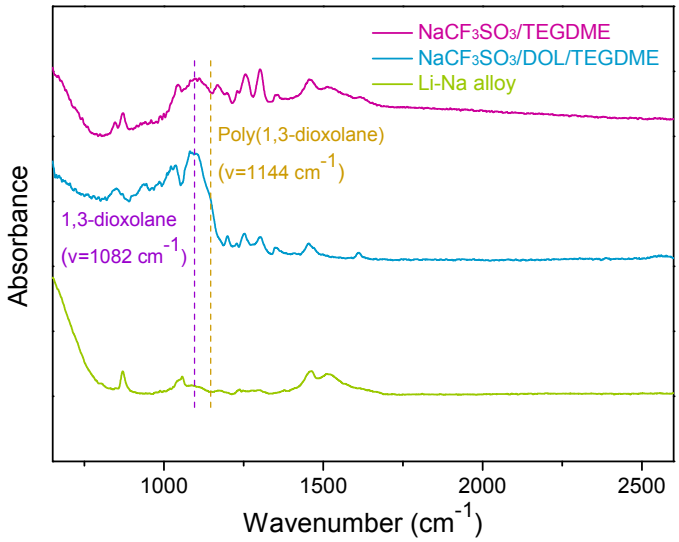

Supplementary Fig. 11. FTIR characterization of SEI on Li-Na alloy anode (Na/Li = 6) cycled in different electrolytes.

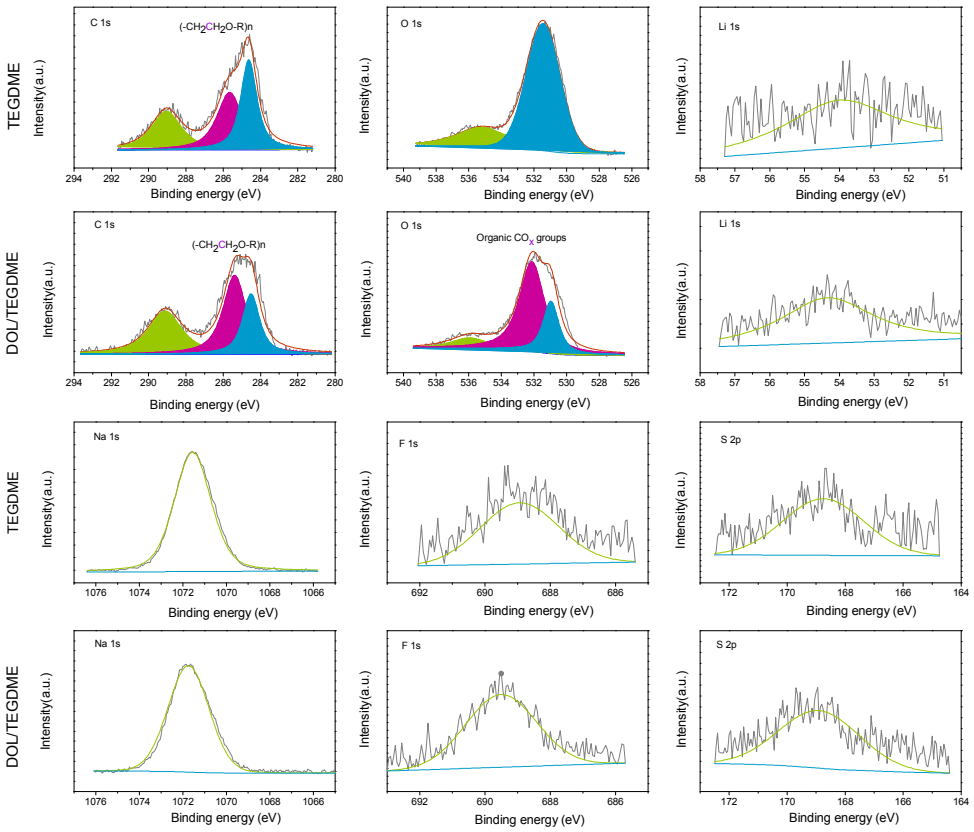

Supplementary Fig. 12. XPS characterization of SEI. C1s, O1s, Li1s, Na1s, F1s, and S2p XPS spectra of SEI on Li-Na alloy (Na/Li = 6) electrodes cycled in different electrolytes.

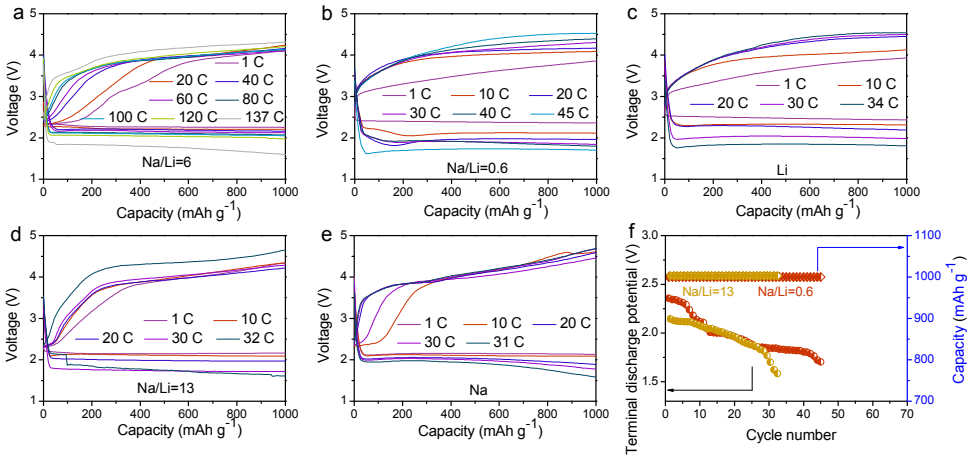

Supplementary Fig. 13. Electrochemistry performances of metal-O_2 batteries. The discharge-charge curves of metal-O_2 batteries with CNT cathode using (**a**) Li-Na alloy (Na/Li = 6), (**b**) Li-Na alloy (Na/Li = 0.6), (**c**) Li, (**d**) Li-Na alloy (Na/Li = 13), (**e**) Na as anode, and (**f**) the cycling performances of Li-Na alloy (Na/Li = 0.6, 13)-O_2 batteries with CNT cathode at a current density of 200 mA g^{-1} under a capacity limitation of 1000 mAh g^{-1} in 0.5 M $NaCF_3SO_3$/DOL/TEGDME electrolyte.

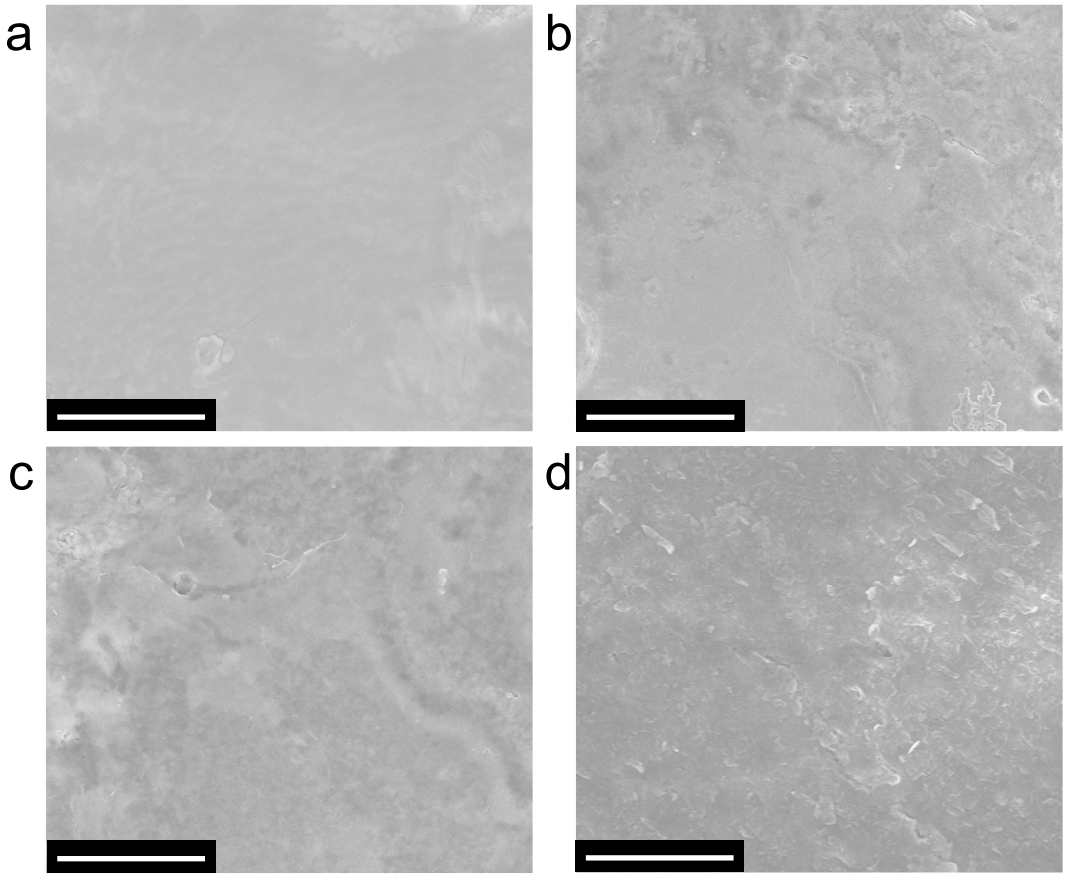

Supplementary Fig. 14. Morphology evolution of Li-Na alloy electrode. SEM images of Li-Na alloy (Na/Li = 6) anodes in Li-Na alloy-O_2 batteries after the (**a**) 1^{st}, (**b**) 40^{th}, (**c**) 80^{th}, and (**d**) 130^{th} cycles. Scale bar, 20 μm.

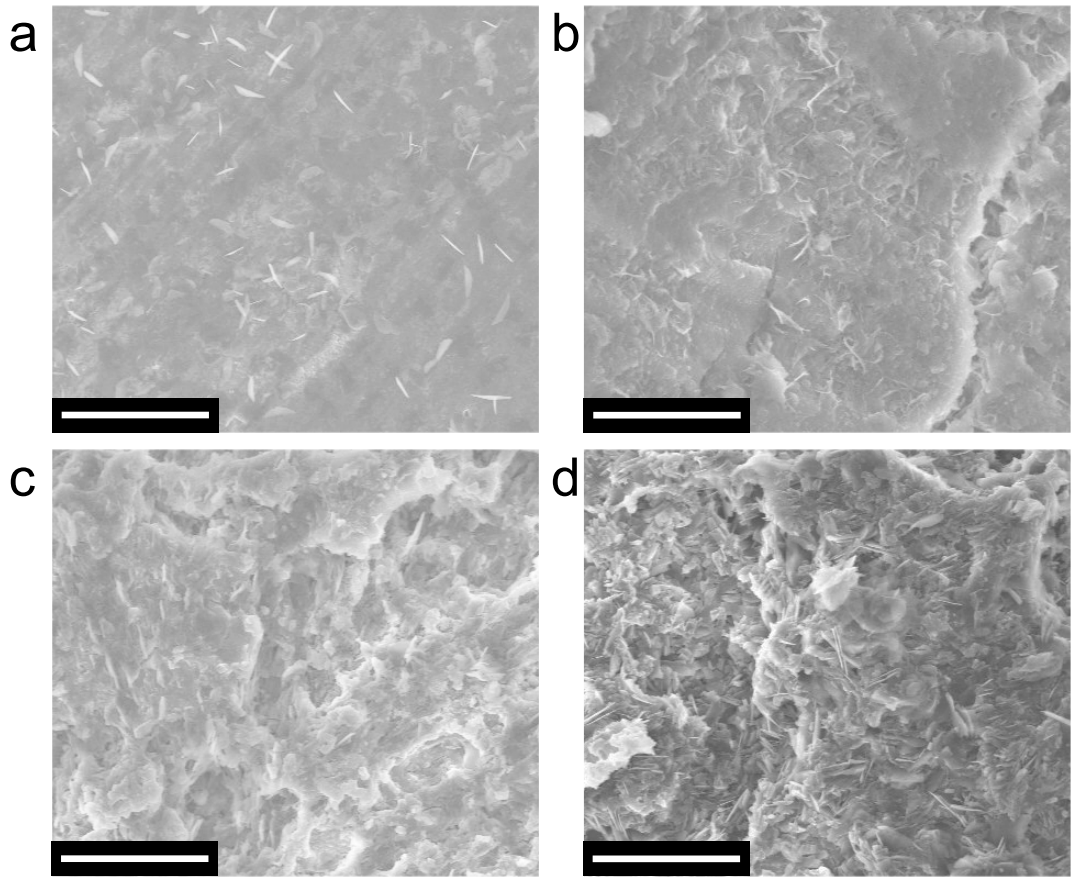

Supplementary Fig. 15. Morphology evolution of Na electrode. SEM images of Na anodes in Na-O_2 batteries after (**a**) 1st, (**b**) 10th, (**c**) 20th, and (**d**) 30th cycles. Scale bar, 20 μm.

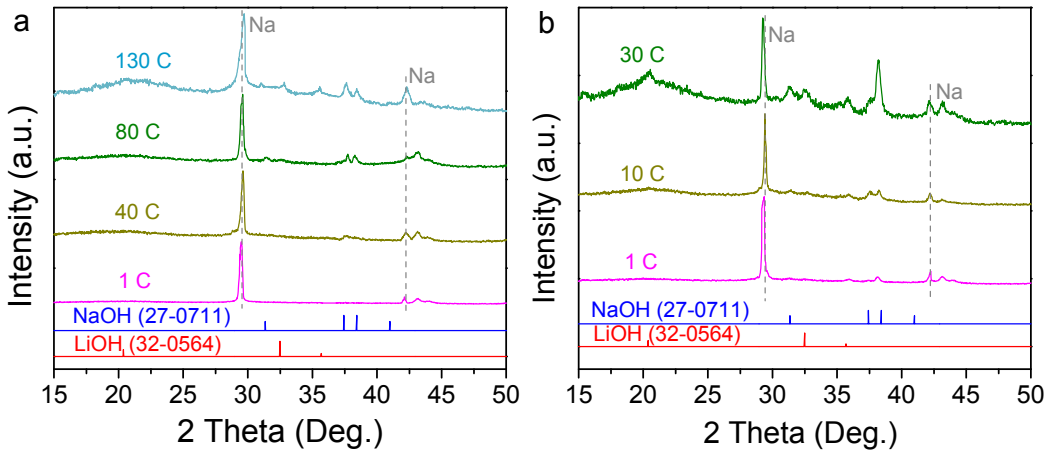

Supplementary Fig. 16. Stability of alloy anodes in different electrolytes. XRD patterns of Li-Na alloy (Na/Li = 6) anode tested under different electrochemical conditions in Li-Na alloy-O_2 batteries with (**a**) 0.5 M $NaCF_3SO_3$/DOL/TEGDME, and (**b**) 0.5 M $NaCF_3SO_3$/TEGDME electrolytes.

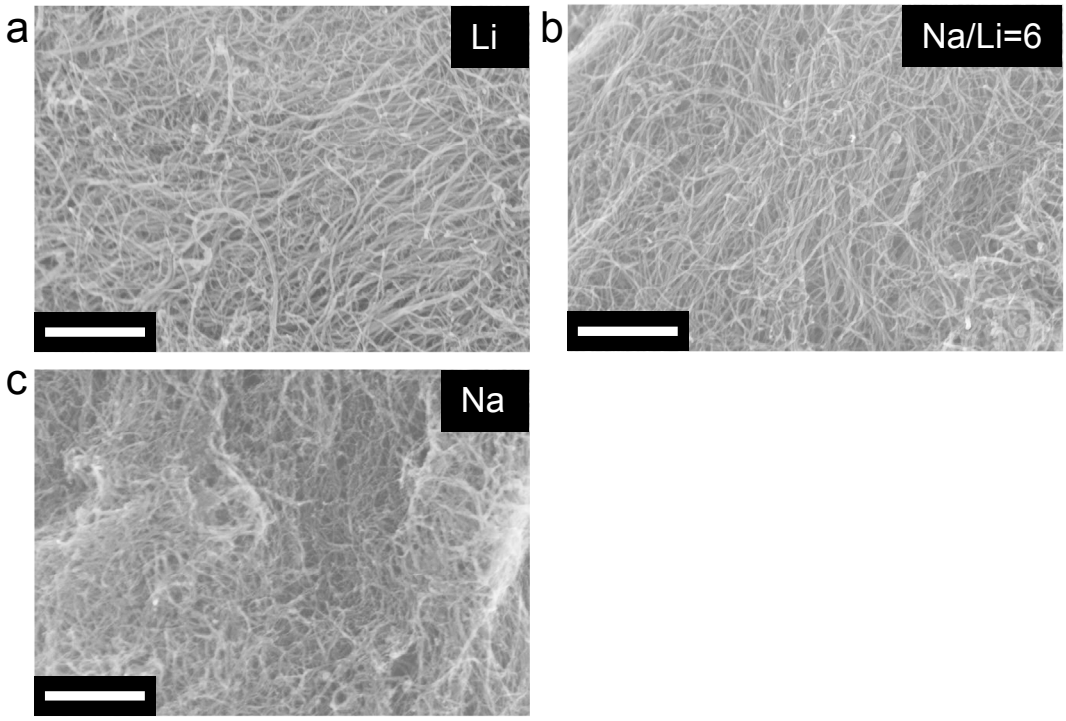

Supplementary Fig. 17. SEM characterizations of discharge products. SEM images of fully charged CNT cathodes of metal-O_2 batteries with (**a**) Li, (**b**) Li-Na alloy (Na/Li = 6), and (**c**) Na anodes. Scale bar, 500 nm.

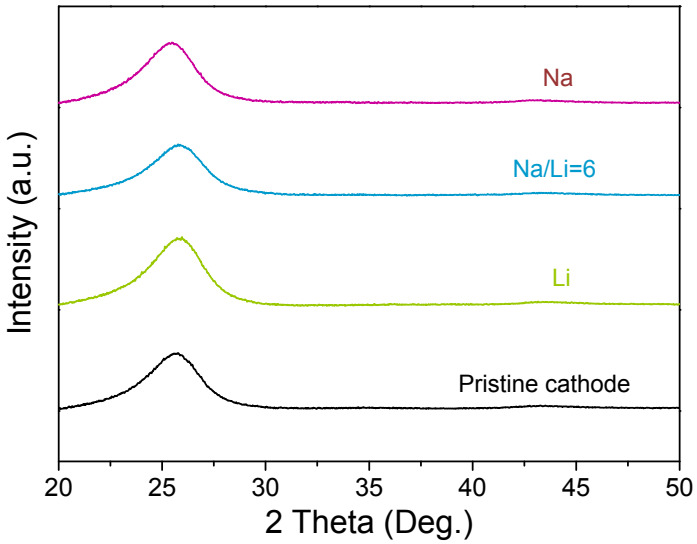

Supplementary Fig. 18. XRD characterizations of discharge products. XRD patterns of fully charged CNT cathodes of metal-O_2 batteries with different metal (Li, Na, Li-Na alloy) anodes.

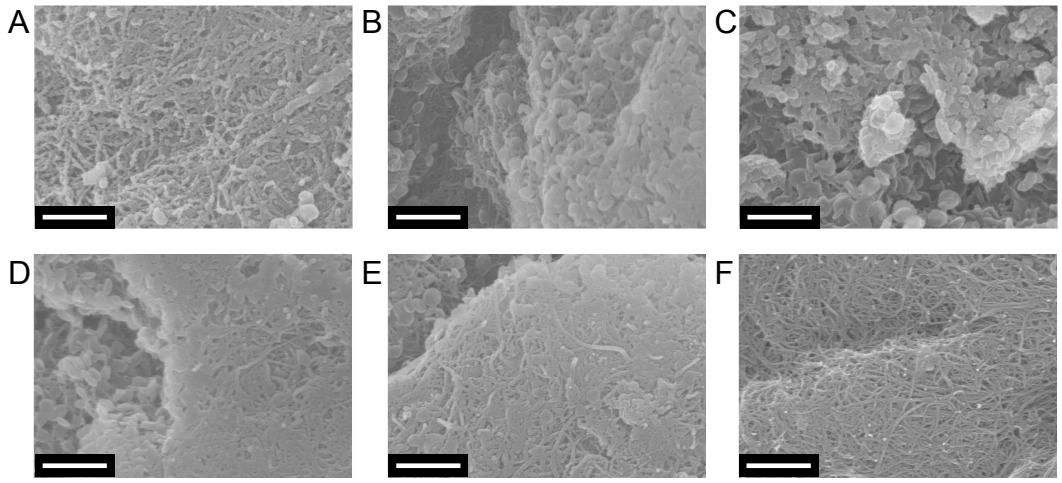

Supplementary Fig. 19. Morphology variation of CNTs electrode during electrochemical process. SEM images show evolution of CNT cathode of an alloy-O_2 battery during the discharge-charge processes, corresponding to positions of the inset of Fig. 5i. Scale bar, 1 μm.

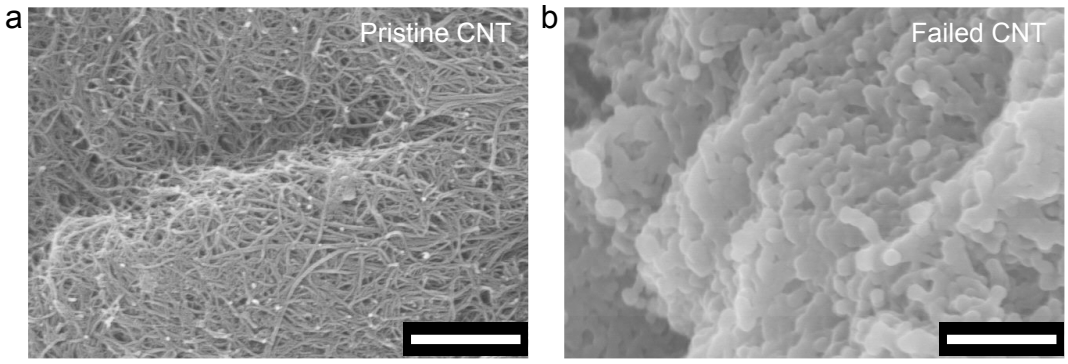

Supplementary Fig. 20. Morphology of CNTs electrode. SEM images for the (**a**) pristine, and (**b**) failed CNTs cathodes.

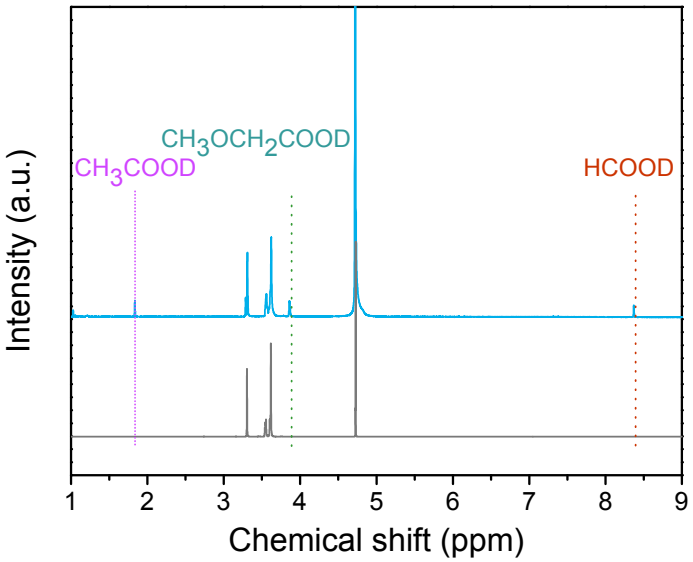

Supplementary Fig. 21. ^{1}H-NMR spectra of side products. ^{1}H-NMR spectra of products on separator from the failed Li-Na alloy-O_2 battery.

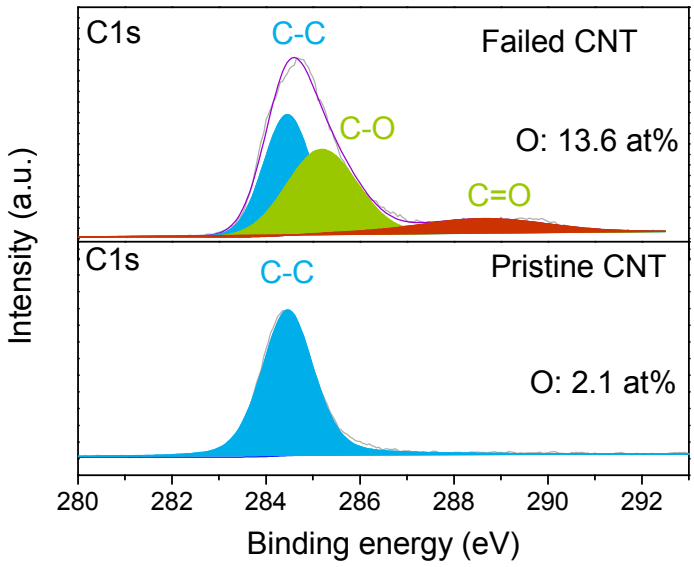

Supplementary Fig. 22. XPS characterizations of CNTs cathode. XPS of C1s spectra of the failed and pristine CNT cathode.

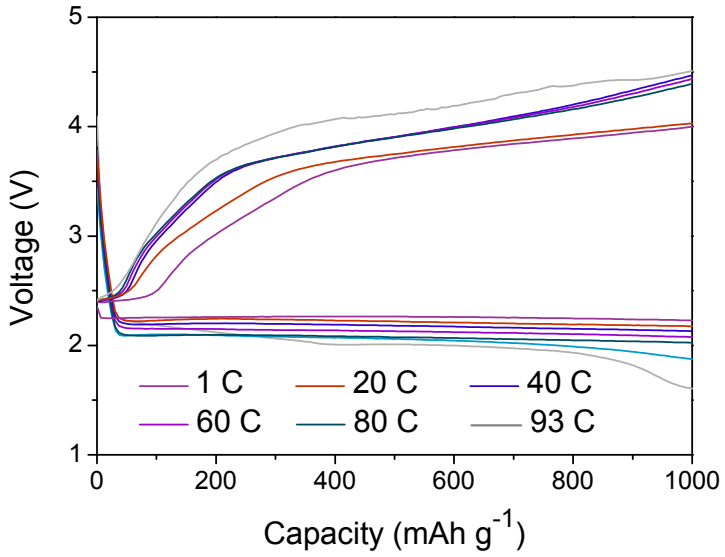

Supplementary Fig. 23. The discharge-charge curves of reassembled Li-Na alloy-O_2 (Na/Li = 6) battery (current density: 200 mA g^{-1}; limited capacity: 1000 mAh g^{-1}).

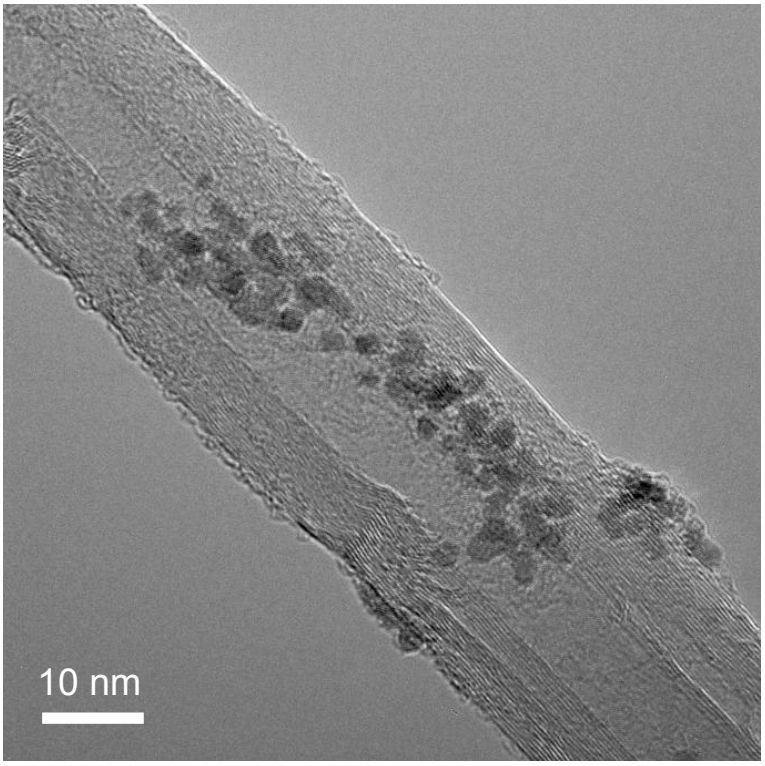

Supplementary Fig. 24. TEM image of RuO_2/CNT catalysts.

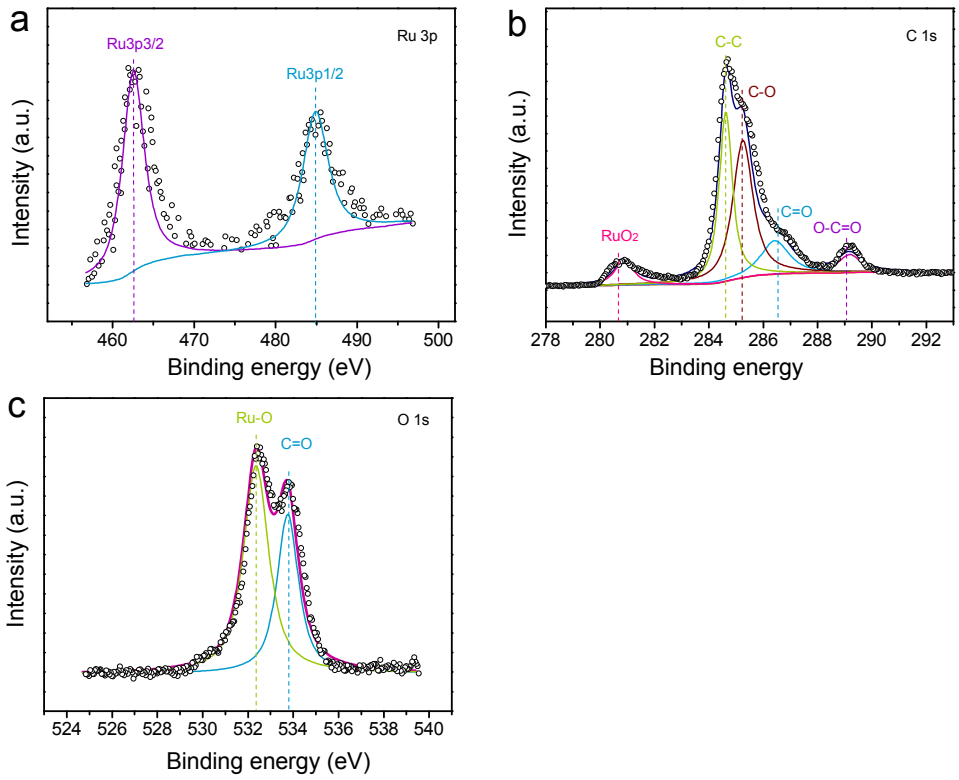

Supplementary Fig. 25. XPS characterizations of RuO_2/CNTs. (**a**) Ru 3p, (**b**) C1s, and (**c**) O1s XPS spectra of RuO_2/CNTs.

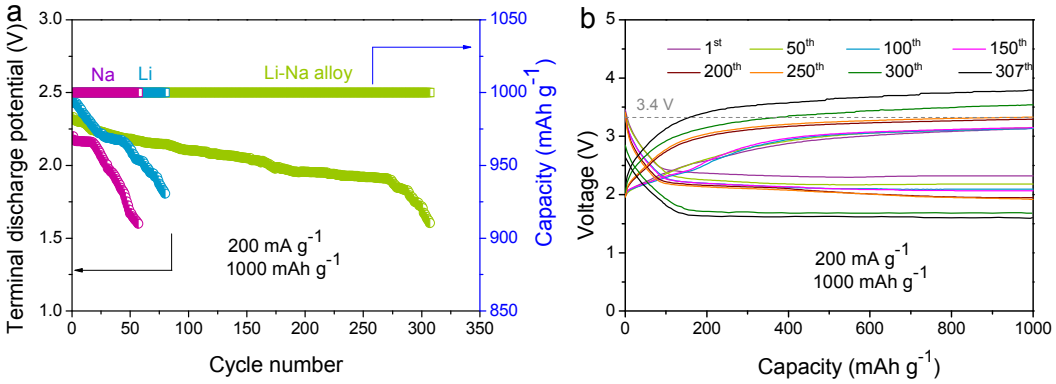

Supplementary Fig. 26. The cycling performance of metal-O_2 batteries. (**a**) The cycling performance of metal-oxygen batteries with Li, Na, and Li-Na alloy (Na/Li = 6) anodes and RuO_2/CNT cathodes. (**b**) The discharge-charge curves of Li-Na alloy (Na/Li = 6)-O_2 batteries.

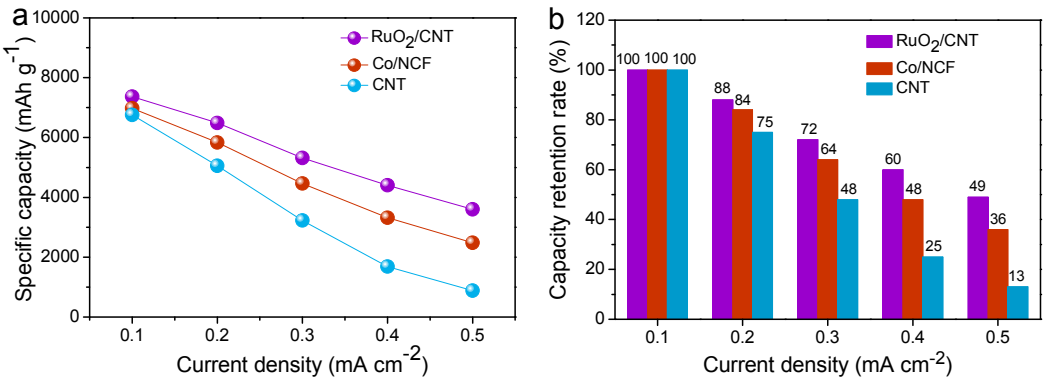

Supplementary Fig. 27. Rate capability of alloy-O_2 batteries with different electrocatalysts. Comparison of a) specific discharge capacity, and b) capacity retention rate of Li-Na alloy (Na/Li = 6) - O_2 batteries with different electrocatalysts at different current densities.

Supplementary Table 1. Preparation parameters of different Li-Na alloys.

Alloy (molar ratio)	Li (g)	Na (g)	Li concentration (at %)	Temperature (K)
Na/Li = 0.6	7.60	14.95	62.5	470
Na/Li = 6	0.76	14.95	14.3	420
Na/Li = 13	0.34	14.95	7.1	390

Supplementary Table 2. Comparison between theoretical and practical discharge potentials of metal-O_2 batteries with different metal anodes.

Anode	Theoretical discharge potential (V)	Practical discharge potential (V)
Li	2.96	2.55
Na/Li = 6	2.42	2.34
Na	2.33	2.13

Supplementary Table 3. Comparison of plating/stripping performance of different Na electrodes.

Electrode	Current density/ mA cm^{-2}	Capacity/ mAh cm^{-2}	Cycling time/ h	Electrolyte	Reference
Al_2O_3-coated Na	0.25	0.125	**450**	1 M $NaClO_4$ EC:DEC (1:1)	[1]
Na@25Al_2O_3	3	1.0	**500**	1 M $NaSO_3CF_3$/DEGDME	[2]
Na	0.3	1.5	**250**	1 M $NaPF_6$/EC/PC (1:1)	[3]
FL-G/Na	0.5	0.5	**200**	1 M $NaPF_6$/EC/DEC (1:1)	[4]
Na-wood	0.5	1.0	**>250**	1 M $NaClO_4$ EC:DEC (1:1)	[5]
Li-Na alloy	0.5	0.5	**860**	0.5 M $NaSO_3CF_3$/DOL/TEGDME	**This work**

Supplementary Table 4. Comparison of electrochemical performances of Na-O_2 batteries with different CNT cathodes.

Cathode	Loading (mg)	Current density (mA g^{-1})	Limited Capacity for Cycling (mAh g^{-1})	Cycle life	Reference
CNT paper	-	500	1000	**< 10**	[6]
NCNTs-CP	8~9	50	100	**< 20**	[7]
NCNTs	0.24~0.36	25	~350	**50**	[8]
CNT powder	0.6	200	1000	**137**	**This work**
RuO_2/ CNTs	0.6	200	1000	**307**	**This work**

1. Luo, W., et al. Ultrathin Surface Coating Enables the Stable Sodium Metal Anode. *Adv. Energy Mater.* **7,** 1601526 (2017).

2. Zhao, Y., et al. Superior Stable and Long Life Sodium Metal Anodes Achieved by Atomic Layer Deposition. *Adv. Mater.* **29,** 1606663 (2017).

3. Song, J., Jeong, G., Lee, A. J., Park, J. H., Kim, H., Kim, Y. J. Dendrite-Free Polygonal Sodium Deposition with Exbatteryent Interfacial Stability in a $NaAlCl_4$-$2SO_2$ Inorganic Electrolyte. *ACS Appl. Mater. Interfaces* **7,** 27206-27214 (2015).

4. Wang, H., Wang, C., Matios, E., Li, W. Critical Role of Ultrathin Graphene Films with Tunable Thickness in Enabling Highly Stable Sodium Metal Anodes. *Nano Lett.* DOI: 10.1021/acs.nanolett.7b03071.

5. Luo, W., et al. Encapsulation of Metallic Na in an Electrically Conductive Host with Porous Channels as a Highly Stable Na Metal Anode. *Nano Lett.* **17,** 3792-3797 (2017).

6. Jian, Z., Chen, Y., Li, F., Zhang, T., Liu, C., Zhou, H. High capacity Na–O_2 batteries with carbon nanotube paper as binder-free air cathode. *J. Power Sources* **251**, 466-469 (2014).

7. Yadegari, H., et al. Three-Dimensional Nanostructured Air Electrode for Sodium-Oxygen Batteries: A Mechanism Study toward the Cyclability of the Battery. *Chem. Mater.* **27**, 3040-3047 (2015).

8. Sun, Q., et al. Self-stacked nitrogen-doped carbon nanotubes as long-life air electrode for sodium-air batteries: Elucidating the evolution of discharge product morphology. *Nano Energy* **12**, 698-708 (2015).